Bootstrapping Multi-atlas Hippocampal Segmentation with MAGeT

Pipitone J., Winterburn J., Lerch J., Pruessner J., Lepage M.,
Voineskos A., Chakravarty M.M., and
the Alzheimer's Disease Neuroimaging Initiative

February 7, 2013

Abstract

Neuroimaging research often relies on automated anatomical segmentations of MR images of the brain. Current multi-atlas based approaches provide accurate segmentations of brain images by propagating manually derived segmentations of specific neuroanatomical structures to unlabelled data. These approaches often rely on a large number of such manually segmented atlases that take significant time and expertise to produce. We present an algorithm for the automatic segmentation of the hippocampus that minimizes the number of atlases needed while still achieving similar accuracy to multi-atlas approaches.

finish

1 Introduction

The hippocampus is of particular interest to many researchers because it is implicated in forms of brain dysfunction such as Alzheimer's disease(Sabuncu et al., 2011) and schizophrenia(Narr et al., 2004; Karnik-Henry et al., 2012), and has functional significance in cognitive processes such as learning and memory(den Heijer et al., 2012; Scoville and Milner, 2000). For many research questions involving magnetic resonance imaging (MRI) data accurate identification of the hippocampus and its subregions is a necessary first step to better understand the individual neuroanatomy of subjects.

Currently, the gold standard for neuroanatomical segmentation is manual delineation by an expert human rater. This is problematic for hippocampal segmentation for several reasons. First, manual segmentation takes a significant investment of time and expertise (Hammers et al., 2003) which may not be readily available to researchers or clinicians. Second, the amount of data produced in neuroimaging experiments increasingly exceeds the capacity for identification of specific neuroanatomical structures by an expert manual rater. Third, the true definition of hippocampal anatomy in MR images is disputed (Geuze et al., 2004), as evidenced by efforts to create an unified segmentation protocol (Jack et al., 2011).

Compounding each of these problems is the significant neuroanatomical variability in the hippocampus throughout the course of aging, maturation, and neuropsychiatric disorders (**?**Sabuncu et al., 2011; **?**; Gogtay et al., 2006; Narr et al., 2002). The result is that existing hippocampal atlases available to a researcher may not accurately represent neuroanatomy of a specific population under study. Additionally, in the course of a research or clinical study, it may be necessary to make adjustments to hippocampal definition as a means of hypothesis testing. For example, Poppenk (Poppenk and Moscovitch, 2011) found that subdividing the hippocampus into anterior and posterior regions resulted in a predictive relationship between volume difference of those regions and recollection memory performance. Making such modifications to a set of MRI data segmentations requires additional manual effort.

Fully-automated segmentation techniques require no human expertise beyond that of initial setup or training. One broad class of automated approach is that of the *model-based* approaches which employ models of anatomical feature variation to constrain segmentations. In this paper we focus on a subclass known as *multi-atlas* approaches which make use of a series of expertly segmented MRIs (the atlas library)

as models to guide the segmentation of a query subject's MRI, and achieve some of the best automated hippocampal segmentation accuracies to-date.

The multi-atlas segmentation technique was pioneered by Heckemann et al. with the MAPER algorithm (Heckemann et al., 2006, 2011). The basic strategy is as follows. Each atlas image is fit a subject's neuroanatomy using nonlinear registration techniques (Collins et al., 1995; Klein et al., 2009). This resulting nonlinear transformation is then applied to the atlas labels to bring them into the subject space. Finally, a *label fusion* technique, such as voxel-wise voting, is used to merge these labels into a definitive segmentation for the subject. Typically, an atlas selection approach is used to improve accuracy by only using labels from atlases that are most similar to a subject image (cross-correlation of image intensities is a common similarity metric) (Aljabar et al., 2009).

Multi-atlas techniques have been applied very successfully to hippocampal segmentation. Collins et al. found that with an atlas library of 80 atlas images, the use of the ANIMAL nonlinear registration algorithm, the normalised mutual information as similarity metric for atlas selection, and majority vote for decision fusion they were able to achieve a mean Dice Kappa similarity score (DSC) to manual labels of 0.886(Collins and Pruessner, 2010). The Alzheimer's Disease Neuroimaging Initiative (ADNI) is a commonly used benchmarking dataset of MR images of controls and patients with MCI or Alzheimer's (see Methods for more information on the ADNI dataset). Leung et al. tuned a multi-atlas approach to the segmentation of ADNI1 1 year dataset of images and using 55 atlases and the STAPLE decision fusion method (Warfield et al., 2004) achieved an mean DSC of 0.89 to the manual segmentations supplied with the ADNI data (Leung et al., 2010). The MAPER whole brain segmentation algorithm (described above), using 30 atlases, achieved a mean DSC score of 0.889 on all ADNI1 baseline images (Heckemann et al., 2011). In (**?**), the authors use a proprietary non-linear registration method based on intensity differences, and post-processing step taking into account these intensity differences to tidy up fused segmentations. Using images from the ADNI1 baseline dataset, they achieved a mean DSC of 0.885 with 30 atlases. With the LEAP algorithm, Wolz et al. explored an elegant modification to the basic strategy: the atlas library is grown, beginning with a set of manually labelled atlases and successively incorporating unlabelled subject images after being labelling using multi-atlas techniques(Wolz et al., 2010). The sequence in which subject images are labelled is chosen so that the similarity between the atlas images and the target images is minimised at each step, effectively allowing for deformations between very dissimilar images to be broken up into sequences of smaller deformations. With an atlas library of 30 MR images, LEAP was used to segment the ADNI1 baseline dataset, achieving a mean Dice score of 0.85 with manual segmentations.

While not purely nulti-atlas techniques, there are several important algorithms for hippocampal segmentation that inform our approach. The popular FreeSurfer application's whole brain segmentation algoritm uses a probabilistic atlas of anatomical and tissue classes along with spatial constraints for class labels encoded using a Markov random field model (Fischl et al., 2002). When segmenting hippocampal subfields, FreeSurfer employs a Bayesian inference algorithm using a probabilistic atlas of anatomical classes as a prior, and a likelihood model of how those classes translate into MR image intensities, both trained on manual segmentations of high resolution MR images (**?**). Yushkevitch et al. describe a semi-automated method for hippocampal subfield segmentation of focal T2 images(**?**). The unlabelled MR image must be manually partitioned into 'head', 'body' and 'tail', and then multi-atlas methods are used to segment the image. Finally, an AdaBoost-based bias correction classifier is trained on texture, spatial location, and intensities of manual segmentations and is applied to fix mislabelled voxels.

Aside from the algorithmic choices used in multi-atlas segmentation, it is natural to ask about how the features of the atlases themselves impact the resulting segmentations. As noted, by choosing atlases ranked most similar to a subject image by voxel intensity profile segmentation accuracy is improved, suggesting that neuroanatomical similarity plays a role(Aljabar et al., 2009). Carmichael et al. explored this directly and found that when using only one atlas the important factors leading to improved accuracy are that the atlas have neuroanatomical features that match the subject, and that the atlas segmentation use the same protocol as the gold-standard (Carmichael et al., 2005). Nestor et al. found that hippocampal segmentation protocols that include more dorsal white-matter and posterior anatomy tended to produce higher overlap and better accuracy at distinguishing disease classes in the ADNI1 1 year dataset (Nestor et al., 2012). These results suggest both atlas library neuroanatomy and delineation protocol play a significant role in the resulting segmentation.

Considered along with our earlier discussion on the difficulty of producing manual segmentations of MR

images and the need for adaptable segmentation definitions in order to conduct research, this presents a real problem of labour and expertise when using existing multi-atlas segmentation methods which rely on relatively large atlas libraries (typically between 30 and 80 atlases). Indeed, it may be especially prohibitive to use these methods in situations where producing a single atlas is challenging (e.g. histology-based atlases, or atlases from very high resolution images). In this paper we address the problem of producing accurate segmentations using small numbers of manually segmented atlases.

Our algorith, called MAGeT brain (*M*ultiple *A*utomatically *Ge*nerated *T*emplates), is an extension to the basic multi-atlas-based segmentation schema(**?**). Principally, we explore the possibility of using a small atlas library to bootstrap a much larger *template library* composed of images taken from the target population. The template library is then used to segment the subjects in a similar fashion to basic multi-atlas segmentation: by label propagation and label fusion. The intuition driving this approach is that by generating a template library we leverage the unique neuroanatomy of subject population on hand to initialize the segmentation process and improve accuracy over direct propagation from the atlas library to unlabelled subjects while also using fewer manually segmented atlases.

The insight of generating a template library is not new. Heckemann et al. compared "indirect" segmentation – taking a single atlas and propagating the labels to intermediate subjects before fusing them in a target image space – to multi-atlas segmentation and found that the indirect approach performed worse (Heckemann et al., 2006). In this paper we continue the same line of investigation but explore the performance when using multiple atlases as well as the effect of different registration and fusion methods.

The LEAP algorithm (Wolz et al., 2010), described above, is another example of indirect segmentation previously explored. LEAP proceeds by iteratively segmenting unlabelled images most similar to the atlas library images and then incorporating the labelled images into the atlas library for future iterations. The novelty explored in our current work is to demonstrate the viability of achieving comparable segmentation accuracy using the basic multi-atlas schema and using significantly fewer manually created atlases.

In previous work (**?**), we applied MAGeT brain to segmentation of the human striatum, globus pallidus, and thalamus using a single histologically-derived atlas. The contribution of the present work is to extend our approach to the human hippocampus and perform a rigorous validation. We first conduct an intensive cross-validation of MAGeT on a pool of 69 MRIs from the ADNI database, comparing the performance of MAGeT against basic multi-atlas segmentation using a range of atlas and template library sizes, registration and fusion methods. We then compare MAGeT segmentations of the entire ADNI screening dataset with those of established automated and manual segmentation techniques. Finally, we compare MAGeT segmentations to those of manual segmentations from a dataset of first episode schizophrenic patient MRIs.

2 Methods

2.1 MAGeT Brain Algorithm

In this paper, we use the term *atlas* to mean any manually segmented MR image, and the term *atlas library* to mean a set of such images. We use the term *template* to refer to any MR image, and associated labelling, used to segment another image, and the term *template library* to refer to a set of such images. An atlas library may be used as a template library but, as we will discuss, a template library may also be composed of images with computer generated labellings.

Make sure we what MAGeT for

reference Chakravarty2

The simplest form of multi-atlas segmentation combines labellings derived from several atlases by way of label fusion (Heckemann et al., 2006). We will refer to this as *basic multi-atlas segmentation*. The primary steps are as follow are: (1) an atlas library and unlabelled MR images are given as input, (2) each atlas image is nonlinearly registered to each unlabelled image, (4) each atlas' labels are propagated via the resulting transformations to the unlabelled image space, and (5) the resulting labels are fused to produce a single, definitive segmentation. The particular registration and voting method used are left unspecified.

The segmentation approach we propose is best understood as an extension of multi-atlas segmentation. MAGeT brain adds a preliminary stage to this process in which the template library is constructed rather than given as input. As before, MAGeT brain accepts an atlas library and unlabelled MR subject images as input. Template library images are selected from subject images. The choice of subjects used in the

template library can be made to reflect the neuroanatomy or demographics of the subject set as a whole (for instance, by sampling equally from cases and controls).

To create the template library, labels from each atlas image are propagated to each template library image via the transformation resulting from a non-linear registration between pair of images. As a result, each template library image has a label from each atlas. Basic multi-atlas segmentation is then used to produce segmentations for the entire set of unlabelled images (including those images used in the template library). Figure 1 describes the MAGeT brain algorithm in pseudocode. Source code can be found at http://github.com/pipitone/MAGeTbrain.

Algorithm 1 Pseudocode for the MAGeT Brain algorithm

```
function BasicMultiAtlasSegmentation(Templates, Subjects)
    for all subject do
        for all template do
            propagate all labels for template to subject space
            store subject labels
        end for
        fuse subject labels
    end for
end function

function MAGeTBrain(Subjects, Atlases, n)
    for i = 1 → n do
        choose a subject to be used as a template
        propagate labels from each atlas to template space
        store the template with all of its labels
    end for
    MultiAtlas(Templates, Subjects)
end function
```

2.2 Subjects

2.2.1 ADNI1 1.5T Screening Dataset

Clinical, demographic and pre-processed T1-weighted MRI used in this paper were downloaded by the authors from the ADNI1 database (adni.loni.ucla.edu) between March 2012 and August 2012. The image dataset download was the "ADNI1:Screening 1.5T" standardized dataset available from ADNI [1] (Wyman et al., 2012). This image collection contains uniformly preprocessed images which have been designated to be the "best" after quality control. All images were acquired using 1.5T scanners (General Electric Healthcare, Philips Medical Systems or Siemens Medical Solutions) at multiple sites using the protocol described in (**?**). Representative 1.5T imaging parameters were TR = 2400ms, TI = 1000ms, TE = 3.5ms, flip angle = 8∘, field of view = 240 x 240mm, a 192 x 192 x 166 matrix (x, y, and z directions) yielding a voxel resolution of 1.25 x 1.25 x 1.2 mm^3. Clinical and demographic data are shown in table **??**.

For a subset of ADNI1 images, labels of the left and right hippocampi are available (herein refered to as SNT labels). Semi-automated hippocampal volumetry was carried out using a commercially available high dimensional brain mapping tool (Medtronic Surgical Navigation Technologies, Louisville, CO), that has previously been validated and compared to manual tracing of the hippocampus (Hsu et al., 2002). Measurement of hippocampal volume is achieved first by placing manually 22 control points as local landmarks for the hippocampus on the individual brain MRI data: one landmark at the hippocampal head, one at the tail, and four per image (i.e., at the superior, inferior, medial and lateral boundaries) on five equally spaced images perpendicular to the long axis of the hippocampus. Second, fluid image transformation is used to match the individual brains to a template brain (Christensen et al., 1997). The pixels corresponding to the hippocampus are then labeled and counted to obtain volumes. This method of hippocampal voluming has a documented reliability of an intraclass coefficient better than .94 (Hsu et al., 2002).

2.2.2 SZ First Episode Patients

include image teristics

[1] http://adni.loni.ucla.edu/methods/mri-analysis/adni-standardized-data/

Table 1: ADNI1 1.5T Screening dataset demographics

	N	CN $N = 229$	LMCI $N = 404$	AD $N = 192$	Combined $N = 825$
Age at baseline Years	825	72.3 75.5 78.5	69.9 74.9 80.4	70.8 75.8 81.0	71.1 75.3 80.0
Sex : Female	825	48% (110)	36% (144)	47% (91)	42% (345)
Education	825	14.0 16.0 18.0	14.0 16.0 18.0	12.0 15.5 16.0	13.0 16.0 18.0
Ethnicity : Unknown	825	1% (3)	1% (4)	1% (2)	1% (9)
Not Hisp/Latino		98% (224)	96% (386)	97% (186)	96% (796)
Hisp/Latino		1% (2)	3% (14)	2% (4)	2% (20)
CDR-SB	825	0.0 0.0 0.0	1.0 1.5 2.0	3.0 4.0 5.0	0.0 1.5 3.0
ADAS 13	816	6.00 9.33 12.33	14.33 18.33 23.00	23.41 28.50 34.00	11.00 17.67 24.00
MMSE	825	29.0 29.0 30.0	26.0 27.0 28.2	22.0 23.0 25.0	25.0 27.0 29.0

a b c represent the lower quartile *a*, the median *b*, and the upper quartile *c* for continuous variables.
N is the number of non–missing values.
Numbers after percents are frequencies.

Table 2: Schizophrenia First Episode Patient Demographics

	N	FEP $N = 81$
Age	80	21 23 26
Gender : M	81	63% (51)
Handedness : ambi	81	6% (5)
left		5% (4)
right		89% (72)
Education	81	11 13 15
SES : lower	81	31% (25)
middle		54% (44)
upper		15% (12)
FSIQ	79	88 102 109

a b c represent the lower quartile *a*, the median *b*, and the upper quartile *c* for continuous variables.
N is the number of non–missing values.
Numbers after percents are frequencies.

Table 3: ANIMAL Registration Parameters

Parameters	Stage 1	Stage 2	Stage 3
Model Blur (FWHM)	8	8	4
Input Blur (FWHM)	8	8	4
Iterations	30	30	10
Step	8x8x8	4x4x4	2x2x2
Sub-Lattice	6	6	6
Lattice Diameter	24x24x24	12x12x12	6x6x6

2.3 Image pre-processing

Before images were registered, the N3 algorithm (Sled et al., 1998) is first used to minimize the intensity nonuniformity in each of the atlases and unlabeled subject images.

2.4 Registration

2.4.1 Automatic Normalization and Image Matching and Anatomical Labeling (ANIMAL)

The ANIMAL algorithm carries out image registration is in two phases. In the first, a 12-parameter linear transformation (3 translations, rotations, scales, shears) is estimated between images using an algorithm that maximizes the correlation between blurred MR intensities and gradient magnitude over the whole brain (Collins et al.). In the second phase, nonlinear registration is completed using the ANIMAL algorithm (Collins et al., 1995): an iterative procedure that estimates a 3D deformation field between two MR images. At first, large deformations are estimated using blurred version of the input data. These larger deformations are then input to subsequent steps where the fit is refined by estimating smaller deformations on data blurred with a Gaussian kernel with a smaller FWHM. The final transformation is a set of local translations defined on a bed of equally spaced nodes that were estimated through the optimization of the correlation coefficient. For the purposes of this work we used the regularization parameters optimized in Robbins et al. (Robbins et al., 2004), displayed in table 3.

2.4.2 Automatic Normalization Tools (ANTS)

ANTs is a diffeomorphic registration algorithm which provides great flexibility over the choice of transformation model, objective function, and the consistency of the final transformation. The transformation is estimated in a hierarchical fashion where the MRI data is subsampled, allowing large deformations to be estimated and successively refined at later hierarchical stages (where the data is subsampled to a finer grid). The deformation field and the objective function are regularized with a Gaussian kernel at each level of the hierarchy. The ANTs algorithm is freely available http://www.picsl.upenn.edu/ANTS/. We used an implementation of the ANTS algorithm compatible with the MINC data format, mincANTS https://github.com/vfonov/mincANTS.

We used the following command line when running the ANTS command,

```
mincANTS 3 -m PR[target_file.mnc,source_file.mnc,1,4]
 --number-of-affine-iterations 10000x10000x10000x10000x10000
 --affine-gradient-descent-option 0.5x0.95x1.e-4x1.e-4
 --use-Histogram-Matching --MI-option 32x16000
 -r Gauss[3,0] -t SyN[0.5] -i 100x100x100x20
 -o transformation.xfm
```

These settings were adapted from the "reasonable starting point" given in the ANTS manual [2].

[2] https://sourceforge.net/projects/advants/files/Documentation/

2.5 Label Fusion

Label fusion is a term given to the process of combining the information from several candidate labellings for an MR image into a single labelling. In this paper we explore the benefits of three different fusion methods.

2.5.1 Voxel-wise Majority Vote

Labels are propagated from all template library images to a subject. Each output voxel is given the most frequent label at that voxel location amongst all candidate labellings. Ties are broken arbitrarily.

2.5.2 Cross-correlation Weighted Majority Vote

An optimal combination of subjects from the template library has previously been shown to improve segmentation accuracy (Aljabar et al., 2009; Collins and Pruessner, 2010). In this method, each template library image is ranked in similarity to each unlabelled image by the normalized cross-correlation (CC) of image intensities after linear registration, over a region of interest (ROI) generously encompassing the hippocampus. Only the top ranked template library image labels are used in a voxel-wise majority vote. The ROI is heuristically defined as the extent of all atlas labels after linear registration to the template, dilated by three voxels (**?**). The number of top ranked template library image labels is a configurable parameter.

The `xcorr_vol` utility from the ANIMAL toolkit is used to calculate the cross-correlation similarity measure.

2.5.3 Normalised Mutual Information Weighted Majority Vote

This method is similar to cross-correlation weighted voting except that image similarity is calculated by the normalised mutual information score over the region of interest(Studholme et al., 2001). The `itk_similarity` utility from the EZMinc toolkit[3] is used to calculate the normalised mutual information measure between to images.

2.6 Overlap Measure

The agreement between two segmentations can assessed using the Dice Similarity Coefficient (DSC):

$$DSC = \frac{2|A \cap B|}{|A| + |B|}$$

where A and B are the regions being compared, and the cardinality is the volume measured in voxels. Using this measure we can compare an automatically generated segmentation to a gold-standard segmentation.

2.7 Experiments

Experiments were performed to assess the performance of MAGeT brain with various parameter settings as well as on diverse datasets. In each experiment we contrast the performance of MAGeT brain with that standard single- and multi-atlas segmentations derived from the same atlas library.

2.7.1 ADNI-1 cross-validation

To test the accuracy of the MAGeT brain algorithm with different parameter settings, repeated random sub-sampling cross-validation (RRSCV) was performed on a subset of the ADNI-1 dataset.

Dataset evaluated. 69 1.5T images were randomly selected from the *ADNI1:Screening 1.5T* standardized dataset. Demographics for this subset are shown in Table 4.

Atlas and template libary. Atlases consisted of images taken from the dataset, with corresponding manual labels provided by SNT. Atlas library size was varied from 3 to 9 images. The remaining images

[3] https://github.com/vfonov/EZminc

Table 4: ADNI-1 cross-validation subset demographics

	CN $N = 23$	LMCI $N = 23$	AD $N = 23$	Combined $N = 69$
Age at baseline Years	72.2 75.5 78.5	71.0 77.1 81.4	71.7 77.8 81.8	71.5 76.6 81.3
Sex : Female	43% (10)	43% (10)	43% (10)	43% (30)
Education	16.0 16.0 18.0	15.0 16.0 18.0	12.0 16.0 16.5	14.0 16.0 18.0
Ethnicity : Unknown	0% (0)	0% (0)	0% (0)	0% (0)
Not Hisp/Latino	100% (23)	100% (23)	100% (23)	100% (69)
Hisp/Latino	0% (0)	0% (0)	0% (0)	0% (0)
CDR-SB	0.00 0.00 0.00	0.75 1.50 1.50	4.00 4.50 5.00	0.00 1.50 4.00
ADAS 13	4.67 5.67 12.34	14.34 16.00 20.50	23.83 29.00 31.66	10.00 16.00 25.33
MMSE	28.5 29.0 30.0	25.0 27.0 28.0	21.0 23.0 24.0	24.0 27.0 29.0

a b c represent the lower quartile *a*, the median *b*, and the upper quartile *c* for continuous variables.
Numbers after percents are frequencies.

were segmented, with the template library size varying from 3 to 20 images. Template library images were selected randomly from the images to be segmented.

Registration method. Both the ANTS and ANIMAL registration methods were used.

Label fusion. Majority vote, cross-correlation weighted majority vote, and Normalized Mutual Information weighted majority vote are used. With the weighted majority vote fusion methods, the number of top labels used in the fusion was varied from 3 to 20 images.

Evaluation. Repeated random sub-sampling cross-validation (RRSCV) consists of repeated trials in which items from the dataset are randomly assigned to a training set or validation set. In each trial, performance on the validation set is measured, and then averaged across all trials.

We performed RRSCV on each combination of parameters listed above: atlas library size, template library size, registration method, and label fusion method. We performed 10 trials per parameter combination. In each validation trial, the training set consisted of the images used as atlases, and the validation set consisted of the images to be segmented. The MAGeT brain algorithm and the basic multi-atlas segmentation procedure were applied to segment the images in the validation set. Additionally, in each trial, the single-atlas segmentation was obtained for each atlas-template.

The gold-standard for the segmentation accuracy of images in the validation set was the SNT manual labels.

show off the ber of registr tions/compar did

2.7.2 ADNI-1 Screening Validation

To test the accuracy of MAGeT brain on a real-world task we segment the entire ADNI-1 dataset using an atlas set that is not representative of the subject set.

comparison a strengths, a l mann2011?

Dataset evaluated. All images from the *ADNI1:Screening 1.5T* standardized dataset.

Atlas and template libary. The atlas library consisted of the entire Winterburn atlas set. The Winterburn atlases are digital segmentations of the hippocampus in five in-vivo 300u isotropic T1-weighted MR scans, and include subfield segmentations for the cornus ammonis (CA) 1, CA4, dentate gyrus, subiculum, and CA 2 and 3 combined. Subjects in the Winterburn atlases range in age from 29-57 years (mean age of 37), and include two males and three females.

The template library consisted of 21 randomly selected images from the ADNI1 data dataset (7 healthy, MCI and AD subjects).

Registration method. ANTS, as it performed best in the cross-validation experiment.

okay to refere whilst still in

Label fusion. Majority vote, as it is simpliest to run and performed equally well in cross-validation experiment.

Evaluation.

Since hippocampal segmentation protocols differ between the ADNI labels and Winterburn atlases, this poses a problem for direct similarity comparisons between labels produced by MAGeT brain and the ADNI labels.

explain why resegment th images with protocol and directly like

Table 5: Multi-atlas means

merge	Atlases	ANTS	ANIMAL
1	3.00	0.81	0.76
2	4.00	0.79	0.75
3	5.00	0.82	0.79
4	6.00	0.82	0.78
5	7.00	0.83	0.80
6	8.00	0.83	0.79
7	9.00	0.84	0.80

To evaluate the performance of MAGeT brain, we correlate our segmentation volumes with manual segmentation volumes, as well as with hippocampal volumes of established automated segmentation methods.

Additionally, we compared classification accuracy of subjects by diagnosis based on hippocampal volume using both the SMT labels and our produced labels.

Include a des
of validation
Note that we
rms `validat`
contrast with
or LDA (Cou
used in LOO
adni/our segr

2.7.3 SZ First Episode Patient Validation

Dataset evaluated. To validate that MAGeT performance generalises to other diseases, we measure the performance using the best parameter settings previous found, on a dataset consiting of first episode schizophrenia patients. .

Also consider
consistency (i
of same subje
ferent field st
la Heckemann

Atlas and template libary. - two different atlas sets: a manual hippocampal segmentation of patients, and Winterburn atlas set.

Registration method. ANTS.

Label fusion. Majority vote.

Evaluation. We validate the FEP-atlas segmentations using Dice's Kappa, and the Winterburn-atlas segmentations by correlating volumes.

Also: group c
expecting sep

2.7.4 Winterburn Atlases Validation

Refer to the
scription abo
just include i

Dataset evaluated. - T1 BRAVO scans of the same subjects included in the Winterburn atlas set. These scans are taken within .... weeks of the scans for the Winterburn atlases.

Atlas and template libary. - Atlas library is Winterburn T1 atlases. Template library consists of all five T1 BRAVOs, plus 15 T1 healthy control images.

Registration method. ANTS

Label fusion. Majority vote.

Evaluation. - Leave one out cross-validation (LOOCV) in which all five subjects are segmented in separate runs of MAGeT brain. In each run, the subject to be segmented is excluded from the Atlas library (so only four atlases are used).

Segmentation accuracy is judged by difference in hippocampal volume.

3 Results

3.1 ADNI-1 Cross-Validation

- find significant improvement over multi-atlas performed with the same parameters. Also, find smoothed performance is monotonically increasing but asymptotic in size of both template and atlas library, with peak performance reached after 15 templates.

Can we statis
capture what
performance
thing like, th
at which gain
statistically i
cant?

Ideas:

- more atlases -¿ better performance
- larger template library -¿ better performance, but tails off around 10-15 templates
- no significant difference between majority or weighted vote methods (haven???t tested this statistically though).
- consistently performs better than average naive performance by XXX
- using ANTS, with a large enough template library (¿12) MAGeT brain performs better than the average multi-atlas approach with the same number of atlases. using ANIMAL, 5 or more atlases needed before boost seen.
- more atlases -¿ smaller template library required to improve on average multi-atlas performance
- discuss variance? best/worst case? –how often do we expect random template library selection to work decently

show cost (in
tions) / bene
off graph: sh
ber of registr
per Kappa?
of manual lab
Kappa?)

3.2 ADNI-1 Screen Validation

Ideas:

- A2A shows that if atlas population strongly(?) represents subject set variability, then free choice from atlas population will produce improvements (we know this b/c of extensive validation trials).
- what about in the case where atlas population doesn???t strongly represent subject set variability (e.g. a priori atlas set)? then, we can use atlas selection to refine atlas set?

Kappa agains
manual rater
explain that

3.3 First Episode Schizophrenic Patients

High volume correlation between Winterburn segmentation volumes and ground truth. (High-ish?) Kappa when using manual segmentations as Atlases.

3.4 Winterburn Atlases Validation

4 Discussion

5 Conclusion

References

P Aljabar, R a Heckemann, a Hammers, J V Hajnal, and D Rueckert. Multi-atlas based segmentation of brain images: atlas selection and its effect on accuracy. *NeuroImage*, 46(3):726–38, July 2009. ISSN 1095-9572. doi: 10.1016/j.neuroimage.2009.02.018. URL http://www.ncbi.nlm.nih.gov/pubmed/19245840.

Owen T Carmichael, Howard A Aizenstein, Simon W Davis, James T Becker, Paul M Thompson, Carolyn Cidis Meltzer, and Yanxi Liu. Atlas-based hippocampus segmentation in Alzheimer's disease and mild cognitive impairment. *NeuroImage*, 27(4):979–90, October 2005. ISSN 1053-8119. doi: 10.1016/j.neuroimage.2005.05.005. URL http://www.pubmedcentral.nih.gov/articlerender.fcgi?artid=2862692&tool=pmcentrez&rendertype=abstract.

G E Christensen, S C Joshi, and M I Miller. Volumetric transformation of brain anatomy. *IEEE transactions on medical imaging*, 16(6):864–77, December 1997. ISSN 0278-0062. doi: 10.1109/42.650882. URL http://ieeexplore.ieee.org/xpl/articleDetails.jsp?arnumber=650882.

D L Collins, P Neelin, T M Peters, and A C Evans. Automatic 3D intersubject registration of MR volumetric data in standardized Talairach space. *Journal of computer assisted tomography*, 18(2):192–205. ISSN 0363-8715. URL http://www.ncbi.nlm.nih.gov/pubmed/8126267.

D Louis Collins and Jens C Pruessner. Towards accurate, automatic segmentation of the hippocampus and amygdala from MRI by augmenting ANIMAL with a template library and label fusion. *NeuroImage*, 52 (4):1355–66, October 2010. ISSN 1095-9572. doi: 10.1016/j.neuroimage.2010.04.193. URL http://www.ncbi.nlm.nih.gov/pubmed/20441794.

D. Louis Collins, C. J. Holmes, T. M. Peters, and A. C. Evans. Automatic 3-D model-based neuroanatomical segmentation. *Human Brain Mapping*, 3(3):190–208, October 1995. ISSN 10659471. doi: 10.1002/hbm.460030304. URL http://doi.wiley.com/10.1002/hbm.460030304.

T den Heijer, F Van der Lijn, M W Vernooij, M de Groot, P J Koudstaal, a Van der Lugt, G P Krestin, a Hofman, W J Niessen, and M M B Breteler. Structural and diffusion MRI measures of the hippocampus and memory performance. *NeuroImage*, 63(4):1782–9, December 2012. ISSN 1095-9572. doi: 10.1016/j.neuroimage.2012.08.067. URL http://www.ncbi.nlm.nih.gov/pubmed/22960084.

Bruce Fischl, David H Salat, Evelina Busa, Marilyn Albert, Megan Dieterich, Christian Haselgrove, Andre van der Kouwe, Ron Killiany, David Kennedy, Shuna Klaveness, Albert Montillo, Nikos Makris, Bruce Rosen, and Anders M Dale. Whole brain segmentation: automated labeling of neuroanatomical structures in the human brain. *Neuron*, 33(3):341–55, January 2002. ISSN 0896-6273. URL http://www.ncbi.nlm.nih.gov/pubmed/11832223.

E. Geuze, E. Vermetten, and J D Bremner. MR-based in vivo hippocampal volumetrics: 2. Findings in neuropsychiatric disorders. *Molecular Psychiatry*, 10(2):160, September 2004. doi: 10.1038/sj.mp.4001579. URL http://www.nature.com.myaccess.library.utoronto.ca/mp/journal/v10/n2/full/4001579a.htmlhttp://www.nature.com.myaccess.library.utoronto.ca/mp/journal/v10/n2/pdf/4001579a.pdf.

Nitin Gogtay, Tom F Nugent, David H Herman, Anna Ordonez, Deanna Greenstein, Kiralee M Hayashi, Liv Clasen, Arthur W Toga, Jay N Giedd, Judith L Rapoport, and Paul M Thompson. Dynamic mapping of normal human hippocampal development. *Hippocampus*, 16(8):664–72, January 2006. ISSN 1050-9631. doi: 10.1002/hipo.20193. URL http://www.ncbi.nlm.nih.gov/pubmed/16826559.

Alexander Hammers, Richard Allom, Matthias J Koepp, Samantha L Free, Ralph Myers, Louis Lemieux, Tejal N Mitchell, David J Brooks, and John S Duncan. Three-dimensional maximum probability atlas of the human brain, with particular reference to the temporal lobe. *Human brain mapping*, 19(4):224–47, August 2003. ISSN 1065-9471. doi: 10.1002/hbm.10123. URL http://www.ncbi.nlm.nih.gov/pubmed/12874777.

Rolf A. Heckemann, Joseph V. Hajnal, Paul Aljabar, Daniel Rueckert, and Alexander Hammers. Automatic anatomical brain MRI segmentation combining label propagation and decision fusion. *NeuroImage*, 46 (3):726–38, July 2006. ISSN 1095-9572. doi: 10.1016/j.neuroimage.2009.02.018. URL http://www.ncbi.nlm.nih.gov/pubmed/19245840.

Rolf A Heckemann, Shiva Keihaninejad, Paul Aljabar, Katherine R Gray, Casper Nielsen, Daniel Rueckert, Joseph V Hajnal, and Alexander Hammers. Automatic morphometry in Alzheimer's disease and mild cognitive impairment. *NeuroImage*, 56(4):2024–37, July 2011. ISSN 1095-9572. doi: 10.1016/j.neuroimage.2011.03.014. URL http://www.pubmedcentral.nih.gov/articlerender.fcgi?artid=3153069&tool=pmcentrez&rendertype=abstract.

Yuan-Yu Hsu, Norbert Schuff, An-Tao Du, Kevin Mark, Xiaoping Zhu, Dawn Hardin, and Michael W Weiner. Comparison of automated and manual MRI volumetry of hippocampus in normal aging and

dementia. *Journal of magnetic resonance imaging : JMRI*, 16(3):305–10, September 2002. ISSN 1053-1807. doi: 10.1002/jmri.10163. URL http://www.pubmedcentral.nih.gov/articlerender.fcgi?artid=1851676&tool=pmcentrez&rendertype=abstract.

Clifford R Jack, Frederik Barkhof, Matt A Bernstein, Marc Cantillon, Patricia E Cole, Charles Decarli, Bruno Dubois, Simon Duchesne, Nick C Fox, Giovanni B Frisoni, Harald Hampel, Derek L G Hill, Keith Johnson, Jean-François Mangin, Philip Scheltens, Adam J Schwarz, Reisa Sperling, Joyce Suhy, Paul M Thompson, Michael Weiner, and Norman L Foster. Steps to standardization and validation of hippocampal volumetry as a biomarker in clinical trials and diagnostic criterion for Alzheimer's disease. *Alzheimer's & dementia : the journal of the Alzheimer's Association*, 7(4):474–485.e4, July 2011. ISSN 1552-5279. doi: 10.1016/j.jalz.2011.04.007. URL http://www.ncbi.nlm.nih.gov/pubmed/21784356.

Meghana S Karnik-Henry, Lei Wang, Deanna M Barch, Michael P Harms, Carolina Campanella, and John G Csernansky. Medial temporal lobe structure and cognition in individuals with schizophrenia and in their non-psychotic siblings. *Schizophrenia research*, 138(2-3):128–35, July 2012. ISSN 1573-2509. doi: 10.1016/j.schres.2012.03.015. URL http://www.ncbi.nlm.nih.gov/pubmed/22542243.

Arno Klein, Jesper Andersson, Babak A Ardekani, John Ashburner, Brian Avants, Ming-Chang Chiang, Gary E Christensen, D Louis Collins, James Gee, Pierre Hellier, Joo Hyun Song, Mark Jenkinson, Claude Lepage, Daniel Rueckert, Paul Thompson, Tom Vercauteren, Roger P Woods, J John Mann, and Ramin V Parsey. Evaluation of 14 nonlinear deformation algorithms applied to human brain MRI registration. *NeuroImage*, 46(3):786–802, July 2009. ISSN 1095-9572. doi: 10.1016/j.neuroimage.2008.12.037. URL http://www.pubmedcentral.nih.gov/articlerender.fcgi?artid=2747506&tool=pmcentrez&rendertype=abstract.

Kelvin K Leung, Josephine Barnes, Gerard R Ridgway, Jonathan W Bartlett, Matthew J Clarkson, Kate Macdonald, Norbert Schuff, Nick C Fox, and Sebastien Ourselin. Automated cross-sectional and longitudinal hippocampal volume measurement in mild cognitive impairment and Alzheimer's disease. *NeuroImage*, 51(4):1345–59, July 2010. ISSN 1095-9572. doi: 10.1016/j.neuroimage.2010.03.018. URL http://www.pubmedcentral.nih.gov/articlerender.fcgi?artid=2873209&tool=pmcentrez&rendertype=abstract.

Katherine L. Narr, Theo G.M. van Erp, Tyrone D. Cannon, Roger P. Woods, Paul M. Thompson, Seonah Jang, Rebecca Blanton, Veli-Pekka Poutanen, Matti Huttunen, Jouko Lönnqvist, Carl-Gustav Standerksjöld-Nordenstam, Jaakko Kaprio, John C. Mazziotta, and Arthur W. Toga. A Twin Study of Genetic Contributions to Hippocampal Morphology in Schizophrenia. *Neurobiology of Disease*, 11(1):83–95, October 2002. ISSN 09699961. doi: 10.1006/nbdi.2002.0548. URL http://dx.doi.org/10.1006/nbdi.2002.0548.

Katherine L Narr, Paul M Thompson, Philip Szeszko, Delbert Robinson, Seonah Jang, Roger P Woods, Sharon Kim, Kiralee M Hayashi, Dina Asunction, Arthur W Toga, and Robert M Bilder. Regional specificity of hippocampal volume reductions in first-episode schizophrenia. *NeuroImage*, 21(4):1563–75, April 2004. ISSN 1053-8119. doi: 10.1016/j.neuroimage.2003.11.011. URL http://www.ncbi.nlm.nih.gov/pubmed/15050580.

Sean M Nestor, Erin Gibson, Fu-Qiang Gao, Alex Kiss, and Sandra E Black. A Direct Morphometric Comparison of Five Labeling Protocols for Multi-Atlas Driven Automatic Segmentation of the Hippocampus in Alzheimer's Disease. *NeuroImage*, November 2012. ISSN 1095-9572. doi: 10.1016/j.neuroimage.2012.10.081. URL http://www.ncbi.nlm.nih.gov/pubmed/23142652.

Jordan Poppenk and Morris Moscovitch. A Hippocampal Marker of Recollection Memory Ability among Healthy Young Adults: Contributions of Posterior and Anterior Segments. *Neuron*, 72(6):931–937, December 2011. ISSN 0896-6273. doi: 10.1016/j.neuron.2011.10.014. URL http://www.sciencedirect.com/science/article/pii/S089662731100924Xhttp://pdn.sciencedirect.com.myaccess.library.utoronto.ca/science?_ob=MiamiImageURL&_cid=272195&_user=994540&_pii=S089662731100924X&_check=y&_origin=article&_zone=toolbar&_coverDate=22-Dec-2011&view=c&originContentFamily=serial&wchp=dGLbVlV-zSkzk&md5=e75d94a1de9d5c31e146f910b38468da/

1-s2.0-S089662731100924X-main.pdfhttp://www.sciencedirect.com.myaccess.library.utoronto.ca/science/article/pii/S089662731100924X.

Steven Robbins, Alan C Evans, D Louis Collins, and Sue Whitesides. Tuning and comparing spatial normalization methods. *Medical image analysis*, 8(3):311–23, September 2004. ISSN 1361-8415. doi: 10.1016/j.media.2004.06.009. URL http://www.ncbi.nlm.nih.gov/pubmed/15450225.

Mert R Sabuncu, Rahul S Desikan, Jorge Sepulcre, Boon Thye T Yeo, Hesheng Liu, Nicholas J Schmansky, Martin Reuter, Michael W Weiner, Randy L Buckner, Reisa a Sperling, and Bruce Fischl. The dynamics of cortical and hippocampal atrophy in Alzheimer disease. *Archives of neurology*, 68(8):1040–8, August 2011. ISSN 1538-3687. doi: 10.1001/archneurol.2011.167. URL http://www.pubmedcentral.nih.gov/articlerender.fcgi?artid=3248949&tool=pmcentrez&rendertype=abstract.

W B Scoville and B Milner. Loss of recent memory after bilateral hippocampal lesions. 1957. *The Journal of neuropsychiatry and clinical neurosciences*, 12(1):103–113, 2000. URL http://www.ncbi.nlm.nih.gov/pubmed/10678523.

J G Sled, a P Zijdenbos, and a C Evans. A nonparametric method for automatic correction of intensity nonuniformity in MRI data. *IEEE transactions on medical imaging*, 17(1):87–97, February 1998. ISSN 0278-0062. doi: 10.1109/42.668698. URL http://www.ncbi.nlm.nih.gov/pubmed/9617910.

C Studholme, E Novotny, I G Zubal, and J S Duncan. Estimating tissue deformation between functional images induced by intracranial electrode implantation using anatomical MRI. *NeuroImage*, 13(4):561–76, April 2001. ISSN 1053-8119. doi: 10.1006/nimg.2000.0692. URL http://www.ncbi.nlm.nih.gov/pubmed/11305886.

Simon K Warfield, Kelly H Zou, and William M Wells. Simultaneous truth and performance level estimation (STAPLE): an algorithm for the validation of image segmentation. *IEEE transactions on medical imaging*, 23(7):903–21, July 2004. ISSN 0278-0062. doi: 10.1109/TMI.2004.828354. URL http://www.pubmedcentral.nih.gov/articlerender.fcgi?artid=1283110&tool=pmcentrez&rendertype=abstract.

Robin Wolz, Paul Aljabar, Joseph V Hajnal, Alexander Hammers, and Daniel Rueckert. LEAP: learning embeddings for atlas propagation. *NeuroImage*, 49(2):1316–25, January 2010. ISSN 1095-9572. doi: 10.1016/j.neuroimage.2009.09.069. URL http://www.pubmedcentral.nih.gov/articlerender.fcgi?artid=3068618&tool=pmcentrez&rendertype=abstract.

Bradley T Wyman, Danielle J Harvey, Karen Crawford, Matt A Bernstein, Owen Carmichael, Patricia E Cole, Paul K Crane, Charles Decarli, Nick C Fox, Jeffrey L Gunter, Derek Hill, Ronald J Killiany, Chahin Pachai, Adam J Schwarz, Norbert Schuff, Matthew L Senjem, Joyce Suhy, Paul M Thompson, Michael Weiner, and Clifford R Jack. Standardization of analysis sets for reporting results from ADNI MRI data. *Alzheimer's & dementia : the journal of the Alzheimer's Association*, October 2012. ISSN 1552-5279. doi: 10.1016/j.jalz.2012.06.004. URL http://www.ncbi.nlm.nih.gov/pubmed/23110865.

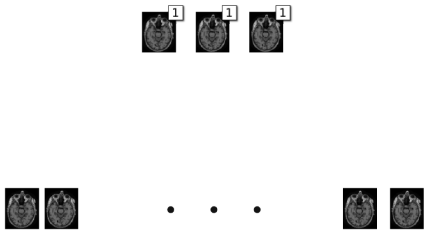

Top row: atlases (with indicators showing that each atlas image has one set of labels).
Bottom row: subject images.

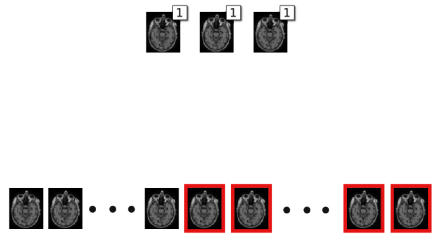

STAGE 1: n template images (in red) are selected arbitrarily from the subjects.

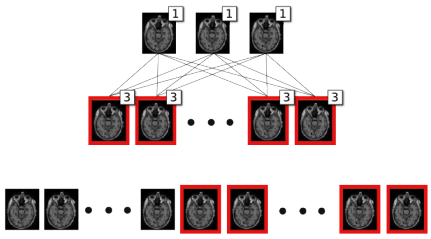

STAGE 3: Labels from the atlases are propagated to the template library.

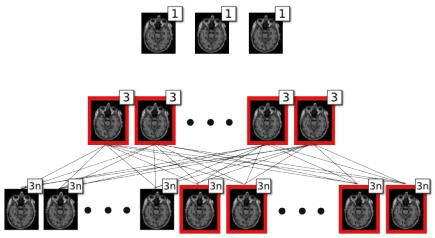

STAGE 4: Labels from the template library are propagated to the subject.
This is much like standard Multi Atlas propagation, except that each
template has multiple labelings (one from each atlas).

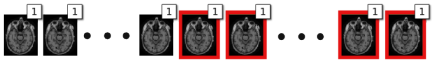

STAGE 5: Subject labels are fused to give a single label for each subject.

Figure 1: Diagram of the MAGeT Brain algorithm

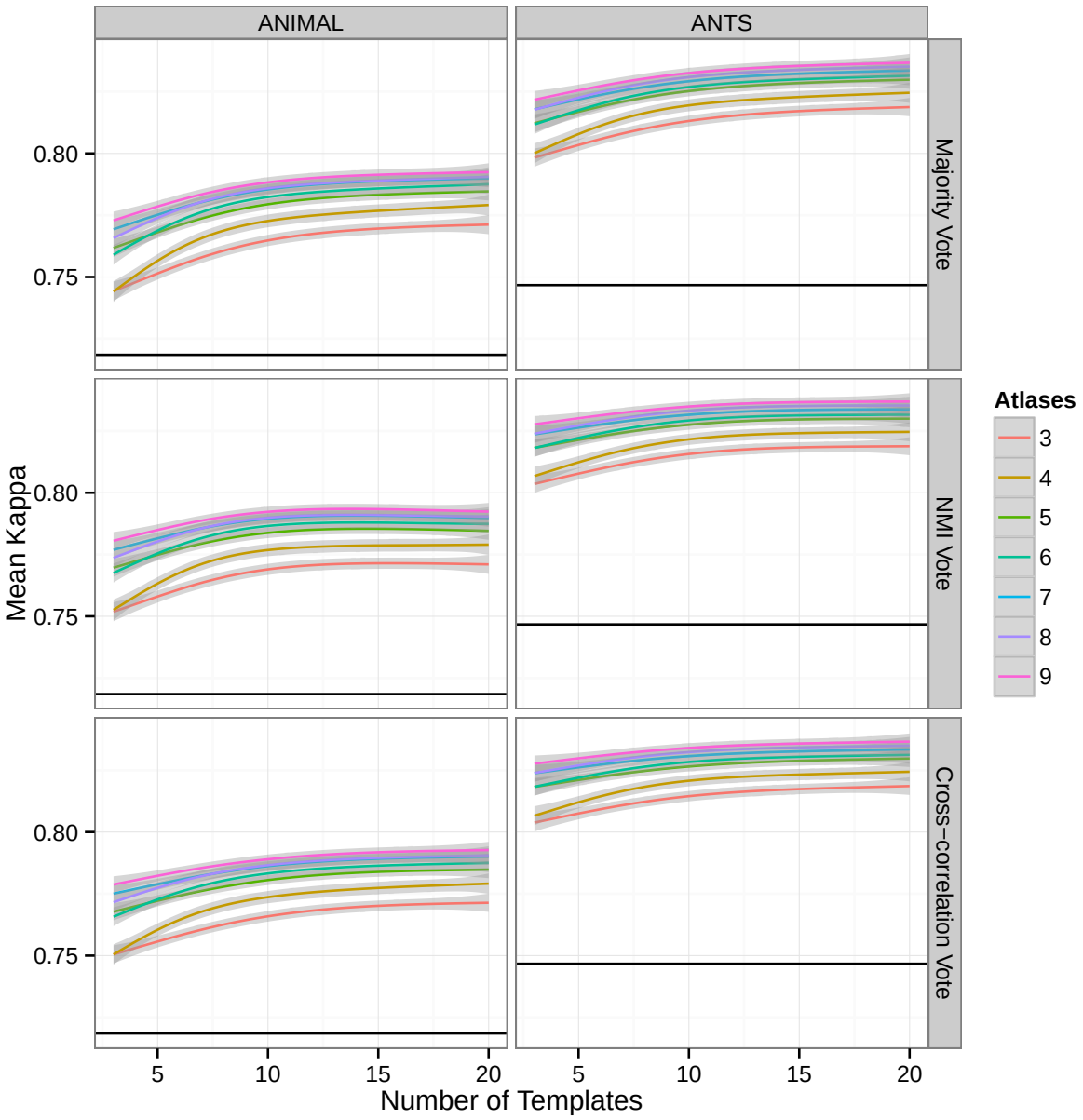

Figure 2: Comparison of MAGeT performance on ADNI-1 subset. Smoothing line fitted using GAM (generalised additive model) from R with defaults from ggplot2 (formula: y s(x, bs = "cs"))

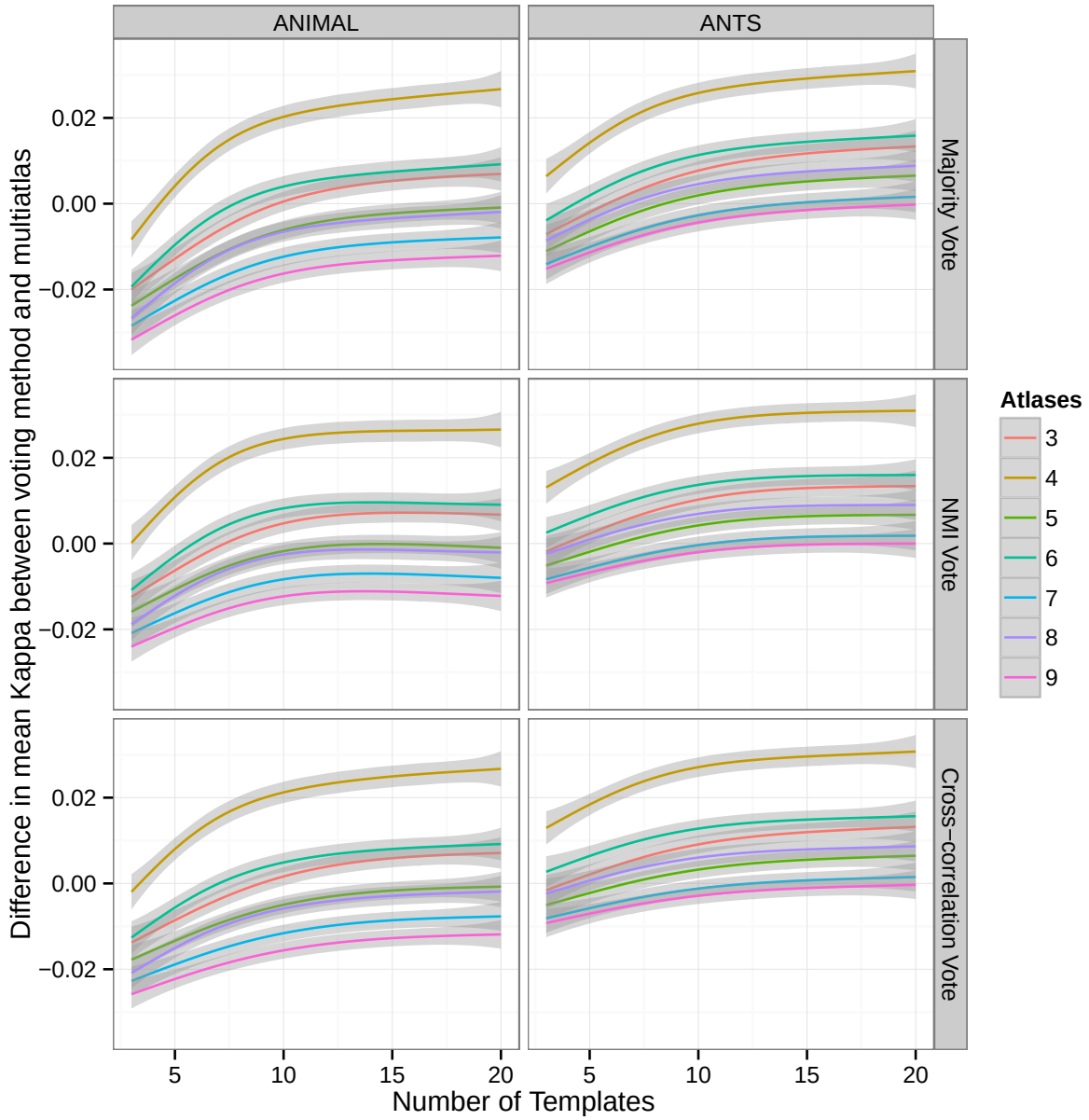

Figure 3: Difference in mean Kappa between MAGeT brain and multi-atlas

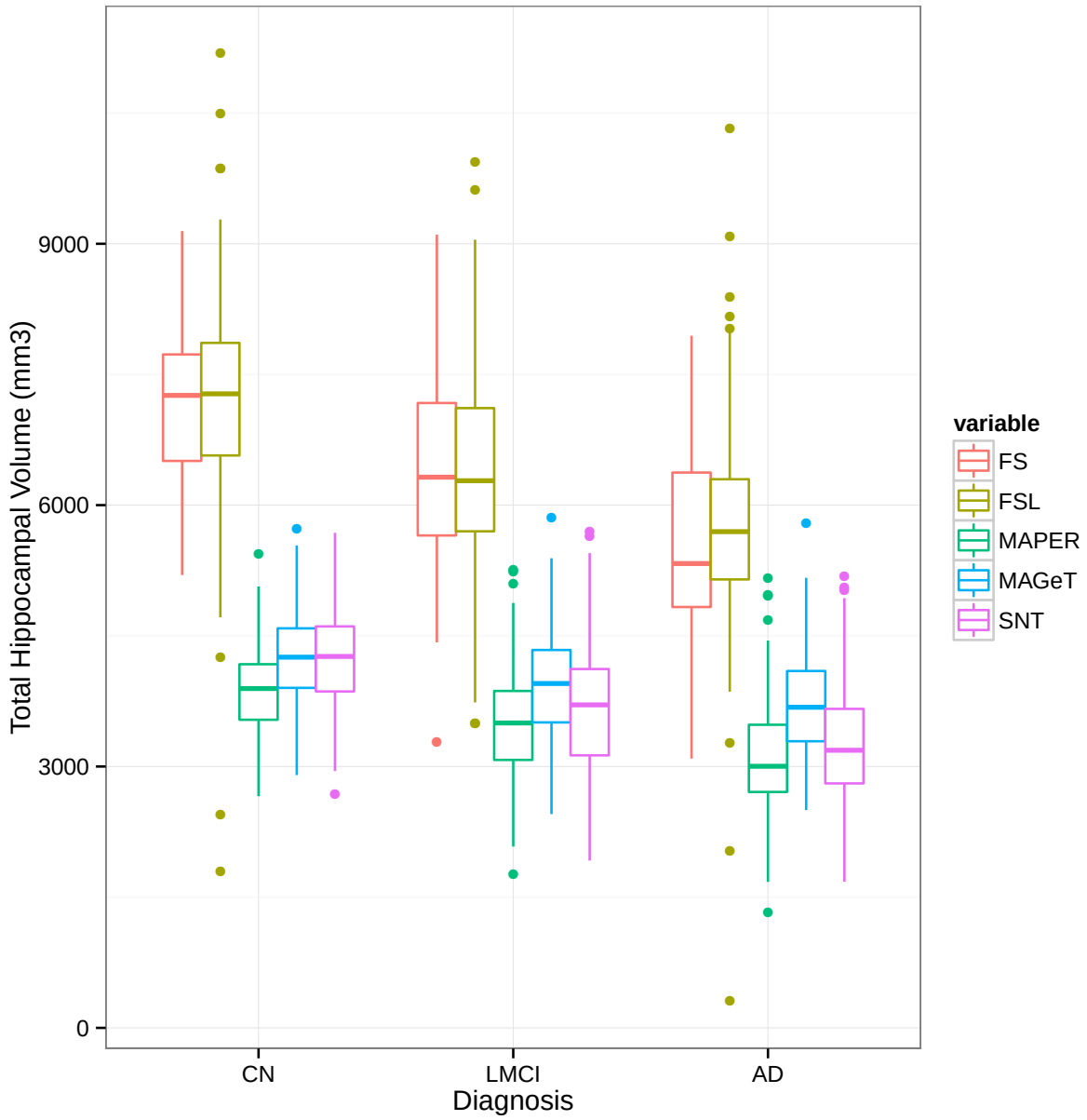

Figure 4: Comparison of HC volumes by FreeSurfer (FSF), MAGeT brain (MAGeT), MAPER, and manual (SNT).

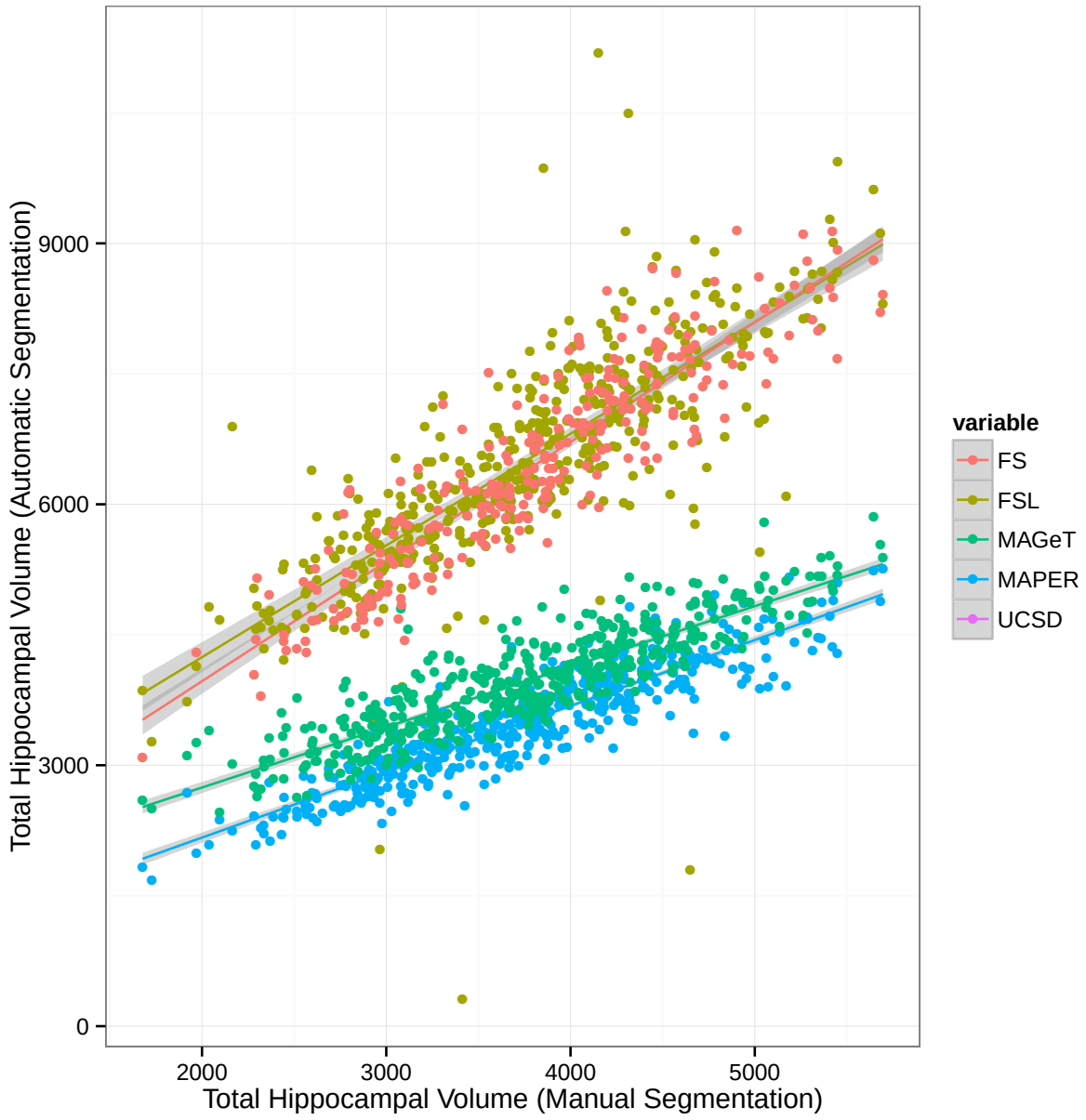

Figure 5: **ADNI Baseline cohort.** Comparison of HC volumes by FreeSurfer (FSF), MAGeT brain (MAGeT), MAPER, and manual (SNT).

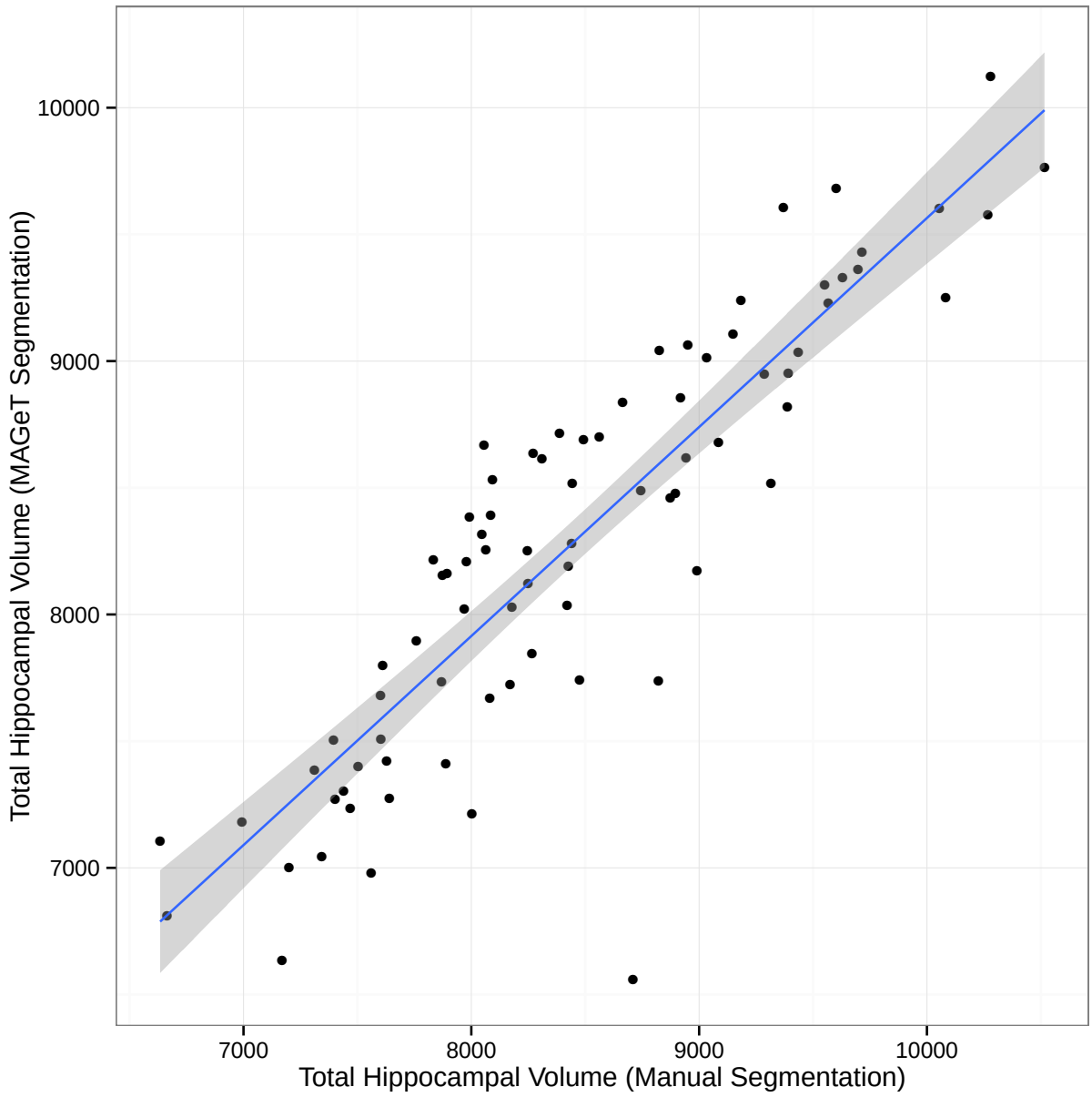

Figure 6: **First Episode Schizophrenic Patients.** Comparison of total HC volumes for MAGeT against manually rated Hippocampal volumes